2

Two-Dimensional Supersonic Flow with Perpendicular Injection of the Gas

Ye. Belyayev[1] and A. Naimanova[2]
[1]*Al-Farabi Kazakh National University,*
[2]*Institute of Mathematics, Ministry of Education and Science, Kazakhstan*

1. Introduction

The flow around jets has been comprehensively studied by many investigators. Mathematical models have been successfully realized for flow of perfect gases [1-4], but the practical design of supersonic ramjet (scramjet) engines requires an understanding of jet interaction with a crossflow for multispecies gases. The flow field in such devices is complicated by geometrical factors, turbulent fuel-air mixing, chemical reaction, shock waves, and separation regions ahead of and behind the jet. Despite successful numerical models of such flows, the detail of the flow physics of the combustion in the real devices through the use of computational tools is a difficult problem. Therefore the investigators studied some physical phenomena or proposed the numerical method which are important for solution of the problem of the combustion.

For example, this problem has been modeled by Drummond and Weidner [1-2] during that process Reynolds-averaged multispecies Navier-Stokes equations which were coupled with Baldwin-Lomax turbulence model have been solved by using the explicit predictor-corrector scheme of MacCormack. Drummond and Weidner modeled injection of fuel from two slots and studied influence of the slots width on the process of mixing. Their comparison of the pressure on the wall to the experiment data showed a satisfactory fit.

Grasso and Magi have also solved the Favre-averaged Navier-Stokes equations for a transverse gas injection in supersonic air streams [4]. The governing equations are solved by a finite volume approach with the $k-\varepsilon$ model equations coupled. A high-order TVD method has been developed to multispecies turbulent gas mixtures and the effect of the free stream Much number on the flow structure have been studied.

The numerical investigation of supersonic mixing of hydrogen with air has been performed in the work [5-6]. For the process the main flow air entering through a finite width of inlet and gaseous hydrogen is injected perpendicularly from the side wall. The explicit TVD scheme has been used to solve the system of two-dimensional Navier-Stokes equations. In this study the enhancement of mixing and good flame-holding capability of a supersonic combustor have been investigated by varying the distance of injector position from left boundary. Upstream recirculation can evolve which might be activated as a good flame holder.

One of the ways to solve Navier-Stokes equation for multispecies flow was proposed by Shuen and Yoon [7], during which they had developed numerical method using high-order

lower-upper symmetric successive overrelaxation scheme. The higher approximation scheme for solution the Favre-averaged Navier- Stokes equations based on the ENO scheme had been constructed in [8-9]. The interaction of a planar supersonic air flow with perpendicularly injected hydrogen jet across the slot from the duct walls have been studied. The influence of the jet Mach number and the ratio of the jet and flow pressure on shock wave structure of the flow and the jet penetration depth was shown.

The $k-\varepsilon$ turbulence model developed by Jones and Launder had been successfully used to numerically calculate supersonic flows [10-11], where the effect of compressibility on the structure of turbulence must be considered. The compressibility correction to the dissipation-rate term in the k transport equation has been used by Rizzeta [10-11] to simulate a supersonic turbulent flowfield.

In this present work, a plane supersonic flow in a channel with perpendicular injection of jets from slots located symmetrically on the lower and upper walls is modeled numerically. For convenience of computations, symmetry is assumed so that only the lower half of the channel is modeled, with jet injection from the lower wall only. The flow pattern is shown in Figure 1.

The influence of the compressibility effect on the shock wave structure and on the vortex system ahead and behind of the jet are studied in the context of the $k-\varepsilon$ and algebraic Baldwin-Lomax models of turbulence. The detailed physical analysis of the supersonic jet interaction with a crossflow for multicomponent gases depending on parameters of the flowfield as the Mach numbers of the air stream, parameters of turbulence, pressure ratio are performed. Such an analysis can improve understanding of the relevant flow structures responsible for the generation of the pressure field and for the mixing of the injectant with the cross flow. Ultimately this analysis will contribute to understanding of scramjet fuel injection systems.

The choice of the range of parameters under consideration is determined by the available experimental data of the processes of hydrogen combustion in the range of regime parameters under consideration, which will allow comparisons with experimental data of other authors in the future.

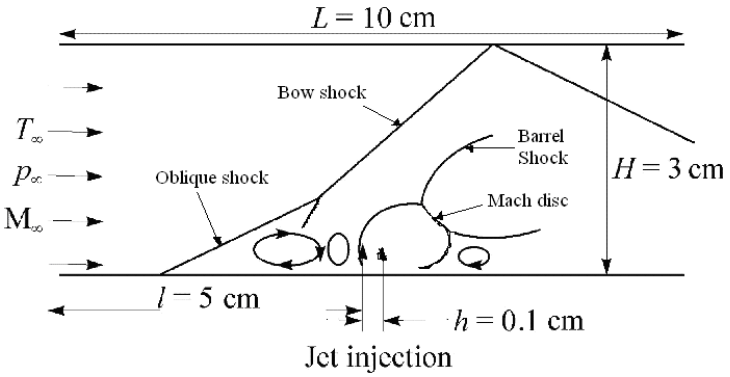

Fig. 1. Two dimensional slot injection flow scheme in the channel. L – length of channel, H – height of channel, l – length from the inlet to the slot, h – slot width.

2. Mathematical model

The two-dimensional Favre-averaged Navier-Stokes equations for multi-species flow with chemical reactions are:

$$\frac{\partial \vec{U}}{\partial t}+\frac{\partial\left(\vec{E}-\vec{E}_v\right)}{\partial x}+\frac{\partial\left(\vec{F}-\vec{F}_v\right)}{\partial z}=0, \tag{1}$$

here the vector of the dependent variables and the vector of fluxes are given as

$$\vec{U}=\begin{pmatrix}\rho\\ \rho u\\ \rho w\\ E_t\\ \rho Y_k\\ \rho k\\ \rho\varepsilon\end{pmatrix}\quad \vec{E}=\begin{pmatrix}\rho u\\ \rho u^2+p\\ \rho uw\\ (E_t+p)u\\ \rho uY_k\\ \rho uk\\ \rho u\varepsilon\end{pmatrix}\quad \vec{F}=\begin{pmatrix}\rho w\\ \rho uw\\ \rho w^2+p\\ (E_t+p)w\\ \rho wY_k\\ \rho wk\\ \rho w\varepsilon\end{pmatrix}$$

$$\vec{E}_v=\left(0,\tau_{xx},\tau_{xz},u\tau_{xx}+w\tau_{xz}-q_x,J_{kx},\frac{1}{\mathrm{Re}}\left(\mu_l+\frac{\mu_t}{\sigma_k}\right)\frac{\partial k}{\partial x},\frac{1}{\mathrm{Re}}\left(\mu_l+\frac{\mu_t}{\sigma_\varepsilon}\right)\frac{\partial \varepsilon}{\partial \mathrm{x}}\right)^T,$$

$$\vec{F}_v=\left(0,\tau_{xz},\tau_{zz},u\tau_{xz}+w\tau_{zz}-q_z,J_{kz},\frac{1}{\mathrm{Re}}\left(\mu_l+\frac{\mu_t}{\sigma_k}\right)\frac{\partial k}{\partial z},\frac{1}{\mathrm{Re}}\left(\mu_l+\frac{\mu_t}{\sigma_\varepsilon}\right)\frac{\partial \varepsilon}{\partial z}\right)^T,$$

The vector of source term is

$$\vec{W}=\left(0,0,0,0,0,\left[P_k-\rho\varepsilon\left(1+\alpha M_t^2\right)+D\right],\left[C_{\varepsilon 1}P_k\varepsilon/k-C_{\varepsilon 2}f_{\varepsilon 2}\rho\varepsilon^2/k+E_\varepsilon\right]\right)^T$$

The stress tensor components, heat and mass fluxes are:

$$\tau_{xx}=\frac{1}{\mathrm{Re}}\left(\mu_l+\frac{\mu_t}{\sigma_k}\right)\left(2u_x-\frac{2}{3}(u_x+w_z)\right);\quad \tau_{zz}=\frac{1}{\mathrm{Re}}\left(\mu_l+\frac{\mu_t}{\sigma_k}\right)\left(2w_z-\frac{2}{3}(u_x+w_z)\right);$$

$$\tau_{xz}=\tau_{zx}=\frac{1}{\mathrm{Re}}\left(\mu_l+\frac{\mu_t}{\sigma_k}\right)(u_z+w_x);$$

$$q_x=\frac{1}{\mathrm{Pr}\,\mathrm{Re}}\left(\mu_l+\frac{\mu_t}{\sigma_k}\right)\frac{\partial T}{\partial x}+\frac{1}{\gamma_\infty M_\infty^2}\sum_{k=1}^{N}h_kJ_{xk};\quad q_z=\frac{1}{\mathrm{Pr}\,\mathrm{Re}}\left(\mu_l+\frac{\mu_t}{\sigma_k}\right)\frac{\partial T}{\partial z}+\frac{1}{\gamma_\infty M_\infty^2}\sum_{k=1}^{N}h_kJ_{zk};$$

$$J_{kx}=-\frac{1}{Sc\,\mathrm{Re}}\left(\mu_l+\frac{\mu_t}{\sigma_k}\right)\frac{\partial Y_k}{\partial x},\quad J_{kz}=-\frac{1}{Sc\,\mathrm{Re}}\left(\mu_l+\frac{\mu_t}{\sigma_k}\right)\frac{\partial Y_k}{\partial z}.$$

Parameters of the turbulence are:

$$P_k = \tau_{txx}\frac{\partial u}{\partial x} + \tau_{txz}\frac{\partial u}{\partial z} + \tau_{tzx}\frac{\partial w}{\partial x} + \tau_{tzz}\frac{\partial w}{\partial z};$$

$$\tau_{txx} = \frac{\mu_t}{\mathrm{Re}}\left(2\frac{\partial u}{\partial x} - \frac{2}{3}\left(\frac{\partial u}{\partial x} + \frac{\partial w}{\partial z}\right)\right);\ \ \tau_{txz} = \frac{\mu_t}{\mathrm{Re}}\left(\frac{\partial u}{\partial z} + \frac{\partial w}{\partial x}\right);$$

$$\tau_{tzz} = \frac{\mu_t}{\mathrm{Re}}\left(2\frac{\partial w}{\partial z} - \frac{2}{3}\left(\frac{\partial u}{\partial x} + \frac{\partial w}{\partial z}\right)\right);$$

$$M_t^2 = 2M_\infty^2\, k / T;$$

$$D = -2\cdot\frac{\mu_l}{\mathrm{Re}}\left[\left(\frac{\partial k^{1/2}}{\partial x}\right)^2 + \left(\frac{\partial k^{1/2}}{\partial z}\right)^2\right];$$

$$E_\varepsilon = -\frac{2\mu_l\cdot\mu_t}{\rho\,\mathrm{Re}^2}\left[\left(\frac{\partial^2 u}{\partial x^2}\right)^2 + \left(\frac{\partial^2 u}{\partial z^2}\right)^2 + \left(\frac{\partial^2 w}{\partial x^2}\right)^2 + \left(\frac{\partial^2 w}{\partial z^2}\right)^2\right];$$

$$f_{\varepsilon 2} = 1 - 0.3\exp\left(-\mathrm{Re}_t^2\right);\ \ \mathrm{Re}_t = \mathrm{Re}\left(\frac{\rho k^2}{\mu_l \varepsilon}\right);$$

$$C_{\varepsilon 1} = 1.44; C_{\varepsilon 2} = 1.92; \sigma_k = 1.0; \sigma_\varepsilon = 1.3,$$

where k, ε are the turbulent kinetic energy and rate of dissipation of turbulent kinetic energy respectively. P_k is turbulence production term, M_t is the turbulence Mach number, D, E_ε are the low-Reynolds number terms, and Y_k is the mass fraction of k^{th} species, $k = 1...N$, where N is the number a component of a mix of gases.
The thermal equation for multi-species gas is:

$$p = \frac{\rho T}{\gamma_\infty M_\infty^2 W}, \qquad W = \left(\sum_{k=1}^{N}\frac{Y_k}{W_k}\right)^{-1}, \qquad \sum_{k=1}^{N} Y_k = 1, \tag{2}$$

where W_k is the molecular weight of the species.
The total energy equation is

$$E_t = \frac{\rho h}{\gamma_\infty M_\infty^2} - p + \frac{1}{2}\rho\left(u^2 + w^2\right) \tag{3}$$

The enthalpy of the gas mixture is calculated according to

$$h = \sum_{k=1}^{N} Y_k h_k,\ \ h_k = h_k^0 + \int_{T_0}^{T} c_{pk}\,dT$$

where h is the specific enthalpy of k^{th} species.
Specific heat at constant pressure for each component c_{pk} is:

$$c_{pk} = C_{pk} / W, \quad C_{pk} = \sum_{i=1}^{5} \overline{a}_{ki} T^{(i-1)}, \quad \overline{a}_{jk} = a_{jk} T_{\infty}^{\,j-1},$$

molar specific heat C_{pk} is given in terms of the fourth degree polynomial with respect to temperature in the JANAF Thermochemical Tables [12].
The system of equations (1) is written in the conservative, dimensionless form. The governing parameters are the entrance parameters at $x = -\infty$, which are the pressure and total energy normalized to $\rho_{\infty} u_{\infty}^2$, the enthalpy normalized to $R_0 T_{\infty} / W_{\infty}$, the molar specific heat normalized to R_0, the turbulence kinetic energy k normalized to u_{∞}^2, the dissipation of turbulence kinetic energy ε normalized to u_{∞}^3 / h and the considered lengths normalized to the slot width h.

3. Transport properties

The coefficient of dynamic viscosity is represented in the form of the sum of μ_l - molecular viscosity and μ_t - turbulent viscosity:

$$\mu = \mu_l + \mu_t \tag{4}$$

The Wilke formula is used to determine the mixture viscosity coefficient by

$$\mu_l = \sum_{i=1}^{N} \frac{\mathrm{X}_i \mu_i}{\Phi_i},$$

where

$$\Phi_i = \sum_{r=1}^{N} \mathrm{X}_r \left[1 + \sqrt{\frac{\mu_i}{\mu_r}} \left(\frac{W_r}{W_i} \right)^{1/4} \right]^2 \left[\sqrt{8} \sqrt{1 + \frac{W_i}{W_r}} \right]^{-1}$$

μ_i is the molecular viscosity of species i, which is defined by following formula [13, p.16]

$$\mu_i = \frac{\mu_{i\infty}}{\mu_{\Lambda\infty}} \sqrt{W_i T_{\infty}}$$

where

$$\mu_{i\infty} = 2.6693 \times 10^{-7} \frac{\sqrt{W_{i\infty} T_{\infty}}}{\sigma_i^2 \, \Omega_i^{(2.2)^*} \left(T_i^* \right)}, \quad \mu_{\Lambda\infty} = \sum_{i=1}^{N} \frac{\mathrm{X}_i \mu_{i\infty}}{\Phi_i} \tag{5}$$

In (5), σ_i is the collision diameter of species i:

$$\sigma_1 = 2.63; \quad \sigma_2 = 3.30; \quad \sigma_3 = 3.5; \quad \sigma_4 = 3.050; \quad \sigma_5 = 0.50; \quad \sigma_6 = 0.560; \quad \sigma_7 = 3.50,$$

where $\Omega_i^{(2.2)^*}$ is the collision integral, T_i^* - kT/ε_i is the reduced temperature, and $\frac{\varepsilon_i}{k}$ is the potential. According to [13, p.17], $\Omega_i^{(2.2)^*}(T_i^*)=1$.
Turbulent viscosity μ_t is defined by using a $k-\varepsilon$ turbulence model

$$\mu_t = C_\mu f_\mu \mathrm{Re}_t \mu_l, \text{ where } C_\mu = 0.09 \tag{6}$$

$$Re_t = Re\left(\frac{\rho k^2}{\mu_l \varepsilon}\right) \quad f_\mu = \exp\left[\frac{-3.4}{\left(1+0.02Re_t\right)^2}\right].$$

4. Initial and boundary conditions

At the entrance:

$$W_k = W_{k\infty},\ p = p_\infty,\ T = T_\infty,\ u = M_\infty\sqrt{\frac{\gamma_\infty R_0 T_\infty}{W_\infty}},\ w = 0,\ Y_k = Y_{k\infty},\ x = 0,\ 0 \le z \le H.$$

k,ε at the entrance:
the k,ε profile at the entrance is defined by using Baldwin-Lomax's algebraic turbulence model for known averaged physical parameters of the flow, where the coefficient of turbulent viscosity contains local velocity gradients in the transverse direction. Making an assumption $P_k/\varepsilon = 1$ we find

$$k = k_\infty,\ k_\infty = \frac{\mu_t P_k}{\rho \mathrm{Re}\sqrt{C_\mu f_\mu}}, \text{ where } P_k = \frac{\mu_t}{\mathrm{Re}}\left(\left(\frac{\partial w}{\partial x}\right)^2 + \frac{4}{3}\left(\frac{\partial w}{\partial z}\right)^2\right)$$

$$\varepsilon = \varepsilon_\infty,\ \varepsilon_\infty = C_\mu f_\mu \mathrm{Re}\left(\frac{\rho k^2}{\mu_t}\right).$$

The boundary layer on the wall is given in the input section, and the velocity profile approximated by power law.
On the slot:

$$W_k = W_{k0},\ p = np_\infty,\ T = T_0,\ w = M_0\sqrt{\frac{\gamma_0 R_0 T_0}{W_0}},\ u = 0,\ Y_k = Y_{k0},\ z = 0,\ L_b \le x \le L_b + h.$$

On the slot for $k-\varepsilon$,

$$k = k_0,\quad k_0 = \frac{3w^2 T_i}{2},$$

where T_i is the jet turbulence intensity. Turbulence energy dissipation is defined by assumption $\mu_t = \mu_l$

$$\varepsilon = \varepsilon_0,\quad \varepsilon_0 = \frac{\rho_0 k_0^2}{53.56\,\mu_l},$$

($n = p_0 / p_\infty$ is the jet pressure ratio, p_0 is the jet pressure, and p_∞ is the flow pressure). On the lower wall the no-slip condition is imposed, for the temperature the adiabatic condition are imposed; on the upper boundary the condition of symmetry is assumed; on the outflow the nonreflecting boundary condition [9] is used.

5. Method of the solution

To take into account the flow in the boundary layer, near the wall, and near the slot, i.e., in regions of high gradients, more accurately, we refine the grid in the longitudinal and transverse directions by the transformations

$$\frac{\partial \tilde{U}}{\partial t} + \frac{\partial \tilde{E}}{\partial \xi} + \frac{\partial \tilde{F}}{\partial \eta} = \frac{\partial \tilde{E}_{v2}}{\partial \xi} + \frac{\partial \tilde{E}_{vm}}{\partial \xi} + \frac{\partial \tilde{F}_{v2}}{\partial \eta} + \frac{\partial \tilde{F}_{vm}}{\partial \eta}, \tag{7}$$

where

$$\tilde{U} = \vec{U}/J,\ \tilde{E} = \xi_x \vec{E}/J,\ \tilde{F} = \eta_z \vec{F}/J,\ \tilde{E}_{v2} = \xi_x \vec{E}_{v2}/J,\ \tilde{E}_{vm} = \xi_x \vec{E}_{vm}/J,\ \tilde{F}_{v2} = \eta_z \vec{F}_{v2}/J,$$
$$\tilde{F}_{vm} = \eta_z \vec{F}_{vm}/J, \text{ and } J = \partial(\xi,\eta)/\partial(x,z)$$

is the Jacobian of mapping..
System (7) linearized with respect to the vector U in form:

$$\tilde{U}^{n+1} + \Delta t\left(\frac{\partial \tilde{E}^{n+1}}{\partial \xi} + \frac{\partial \tilde{F}^{n+1}}{\partial \eta} - \frac{\partial \tilde{E}_{vm}^{n+1}}{\partial \xi} - \frac{\partial \tilde{E}_{v2}^{n+1}}{\partial \xi} - \frac{\partial \tilde{F}_{vm}^{n+1}}{\partial \eta} - \frac{\partial \tilde{F}_{v2}^{n+1}}{\partial \eta}\right) =: \tilde{U}^n + O\left(\Delta t^2\right). \tag{8}$$

Here,

$$\tilde{E}^{n+1} \approx A_\xi^n \tilde{U}^{n+1},\quad \tilde{F}^{n+1} \approx B_\eta^n \tilde{U}^{n+1}, \tag{9}$$

$$A_\xi = \xi_x A,\quad B_\eta = \eta_z B,$$

where $A = \partial \vec{E} / \partial \vec{U}$ and $B = \partial \vec{F} / \partial \vec{U}$ are the Jacobian matrices [8-9].
The terms containing the second derivatives are presented as sums of two vectors:

$$\tilde{E}_{v2}^{n+1} = \tilde{E}_{v21}^{n+1} + \tilde{E}_{v22}^{n},\quad \tilde{F}_{v2}^{n+1} = \tilde{F}_{v21}^{n+1} + \tilde{F}_{v22}^{n}, \tag{10}$$

where the vectors $\tilde{E}_{v21}^{n+1}$, $\tilde{F}_{v21}^{n+1}$ are written in the following form:

$$\tilde{E}_{v11}^{n+1} = \frac{\mu_t \xi_x}{\mathrm{ReJ}}\left[0, \frac{4}{3}\frac{\partial}{\partial \xi}\left(\frac{u\ \rho}{\rho}\right)^{n+1}, \frac{\partial}{\partial \xi}\left(\frac{w\ \rho}{\rho}\right)^{n+1}, \frac{\gamma}{\mathrm{Pr}}\frac{\partial}{\partial \xi}\left(\frac{E_t}{\rho}\right)^{n+1}\right]^T,$$

$$\tilde{F}_{v21}^{n+1} = \frac{\mu_t \eta_z}{\mathrm{ReJ}}\left[0, \frac{\partial}{\partial \eta}\left(\frac{u\ \rho}{\rho}\right)^{n+1}, \frac{4}{3}\frac{\partial}{\partial \eta}\left(\frac{w\ \rho}{\rho}\right)^{n+1}, \frac{\gamma}{\mathrm{Pr}}\frac{\partial}{\partial \eta}\left(\frac{E_t}{\rho}\right)^{n+1}\right]^T,$$

and the vectors $\tilde{E}^{n}_{v12}$, $\tilde{F}^{n}_{v22}$ contain the remaining dissipative functions of the form:

$$\tilde{E}^{n}_{v12} = \frac{\xi_x^2}{\mathrm{ReJ}}\left[0,0,0,\left[\left(\mu_t - \frac{\gamma\mu_t}{\mathrm{Pr}}\right)\left(w\frac{\partial w}{\partial \xi}\right) + \left(\frac{4}{3}\mu_t - \frac{\gamma\mu_t}{\mathrm{Pr}}\right)u\frac{\partial u}{\partial \xi}\right]^{n}\right]^{T},$$

$$\tilde{F}^{n}_{v22} = \frac{\eta_z^2}{\mathrm{ReJ}}\left[0,0,0,\left[\left(\mu_t - \frac{\gamma\mu_t}{\mathrm{Pr}}\right)\left(u\frac{\partial u}{\partial \eta}\right) + \left(\frac{4}{3}\mu_t - \frac{\gamma\mu_t}{\mathrm{Pr}}\right)w\frac{\partial w}{\partial \eta}\right]^{n}\right]^{T},$$

$$\tilde{E}_{vm} = \frac{\xi_x\mu_t}{\mathrm{ReJ}}\left[0,-\frac{2}{3}\left(\eta_z\frac{\partial w}{\partial \eta} + \zeta_y\frac{\partial v}{\partial \zeta}\right),\eta_z\frac{\partial u}{\partial \eta},-\frac{2}{3}\left(\zeta_y u\frac{\partial v}{\partial \zeta} + \eta_z u\frac{\partial w}{\partial \eta}\right) + \right.$$
$$\left. + \left(\eta_z w\frac{\partial u}{\partial \eta} + \zeta_y v\frac{\partial u}{\partial \zeta}\right)\right],$$
$$\tilde{F}_{vm} = \frac{\eta_z\mu_t}{\mathrm{ReJ}}\left[0,\eta_z\frac{\partial w}{\partial \eta},-\frac{2}{3}\left(\xi_x\frac{\partial u}{\partial \xi} + \zeta_y\frac{\partial w}{\partial \zeta}\right),\left(\xi_x u\frac{\partial w}{\partial \xi} + \zeta_y u\frac{\partial w}{\partial \zeta}\right) - \right.$$
$$\left. - \frac{2}{3}\left(\xi_x w\frac{\partial u}{\partial \xi} + \zeta_y w\frac{\partial v}{\partial \zeta}\right)\right].$$

According to a principle of construction ENO scheme the system (7) for integration on time is formally represented as:

$$\Delta\tilde{U}^{n+1} + \Delta t\left[\left(\hat{A}^{+} + \hat{A}^{-}\right)\frac{\vec{E}^{m}}{\xi} + \left(\hat{B}^{+} + \hat{B}^{-}\right)\frac{\vec{F}^{m}}{\eta} - \right.$$
$$\left.\left[\frac{(\tilde{E}_{v2}{}^{n+1} + \tilde{E}_{vm}{}^{n})}{\xi} - \frac{(\tilde{F}_{v2}{}^{n+1} + \tilde{F}_{vm}{}^{n})}{\eta}\right]\right] = O\left(1/2\,\Delta t^{2}\right) \tag{11}$$

Here $\vec{E}^{m}$, $\vec{F}^{m}$ is called the modified flux vector. It consists from the original flux vector ($\tilde{E}$, $\tilde{F}$ and additional terms of third-order accuracy $\vec{E}_{\xi},\vec{D}_{\xi}$, $\vec{E}_{\eta},\vec{D}_{\eta}$):

$$\vec{E}^{m} = \tilde{E}^{n+1} + (\vec{E}_{\xi} + \vec{D}_{\xi})^{n}\ , \tag{12}$$

modified flux $\vec{F}^{m}$ is written similarity and $\hat{A}^{+} + \hat{A}^{-} = I$, $\hat{A}^{\pm} = A^{\pm}A^{-1}$, $\hat{B}^{\pm} = B^{\pm}B^{-1}$, I - unity matrix.

Applying factorization to (11), we obtain two one-dimensional operators, which are resolved by matrix sweep:

Step 1.

$$\left[I + \Delta t\left\{(\hat{A}^{+}_{i-1/2}\Delta_{-}A^{n}_{\xi} + \hat{A}^{-}_{i+1/2}\Delta_{+}A^{n}_{\xi}) + \Delta\frac{\mu_t\xi_x^2}{\mathrm{Re}\,J}\Delta\frac{1}{U_1^{n}}\right\}\right]\mathrm{U}^{*} = RHS^{n}_{\xi} + RHS^{n}_{\eta}$$

Step 2.

$$\left[I + \Delta t\left\{(\hat{B}^{+}_{j-1/2}\Delta_{-}B^{n}_{\eta} + \hat{B}^{-}_{j+1/2}\Delta_{+}B^{n}_{\eta}) + \Delta\frac{\mu_t\eta_z^2}{\mathrm{Re}\,J}\Delta\frac{1}{U_1^{n}}\right\}\right]\tilde{\mathrm{U}}^{n+1} = \mathrm{U}^{*}\ , \tag{13}$$

$$RHS_{\xi}^{n} = \hat{A}^{-}_{i+1/2j}\left[\left(\vec{E}_{\xi}+\vec{D}_{\xi}\right)_{i+1j} - \left(\vec{E}_{\xi}+\vec{D}_{\xi}\right)_{ij} \right]^{n} + \hat{A}^{+}_{i-1/2j}\left[\left(\vec{E}_{\xi}+\vec{D}_{\xi}\right)_{ij} - \left(\vec{E}_{\xi}+\vec{D}_{\xi}\right)_{i-1j} \right]^{n},$$

$$\hat{A}^{-}_{i+1/2j}\left[\left(\vec{E}_{\zeta}+\vec{D}_{\zeta}\right)_{ij} \right]^{n} = \left(\boldsymbol{minmod}\left(\overline{E}_{\xi i+1/2j}\, \overline{E}_{\xi i-1/2j}\right) + \right.$$

$$\left. + \begin{cases} \dot{\boldsymbol{m}}\left(\Delta_{-}\hat{D}_{\xi i+1/2j},\, \Delta_{+}\hat{D}_{\xi i+1/2j}\right) & \text{if} \quad \left|\Delta_{-}\tilde{U}_{ij}\right| > \left|\Delta_{+}\tilde{U}_{ij}\right| \\ \dot{\boldsymbol{m}}\left(\Delta_{-}\overline{D}_{\xi i-1/2j},\, \Delta_{+}\overline{D}_{\xi i-1/2j}\right) & \text{if} \quad \left|\Delta_{-}\tilde{U}_{ij}\right| \le \left|\Delta_{+}\tilde{U}_{ij}\right| \end{cases} \right),$$

$$\hat{A}^{+}_{i-1/2j}\left[\left(\vec{E}_{\xi}+\vec{D}_{\xi}\right)_{ij} \right]^{n} = R\,\hat{\Lambda}^{+}\,R^{-1}_{i-1/2j}\left[\left(\boldsymbol{minmod}\left(\overline{E}_{\xi i+1/2j}\, \overline{E}_{\xi i-1/2j}\right) - \right.\right.$$

$$\left.\left. - \begin{cases} \dot{\boldsymbol{m}}\left(\Delta_{-}\hat{D}_{\xi i-1/2j},\, \Delta_{+}\hat{D}_{\xi i-1/2j}\right) & \text{if} \quad \left|\Delta_{-}\tilde{U}_{ij}\right| \le \left|\Delta_{+}\tilde{U}_{ij}\right| \\ \dot{\boldsymbol{m}}\left(\Delta_{-}\overline{D}_{\xi i-1/2j},\, \Delta_{+}\overline{D}_{\xi i-1/2j}\right) & \text{if} \quad \left|\Delta_{-}\tilde{U}_{ij}\right| \le \left|\Delta_{+}\tilde{U}_{ij}\right| \end{cases} \right)\right],$$

$$\overline{E}_{\xi i\pm1/2j} = \left(R\,sign(\Lambda)\,R^{-1}\right)_{i\pm1/2j}\frac{1}{2}\left[I - \frac{\Delta t}{\Delta\xi}\left(R\,|\Lambda|\,R^{-1}\right)_{i\pm1/2}\right]\Delta_{\pm}\tilde{E}_{ij},$$

$$\overline{D}_{\xi i\pm1/2j} = \left(R\,sign(\Lambda)\,R^{-1}\right)_{i\pm1/2j}\frac{1}{6}\left[\frac{\Delta t^{2}}{\Delta\xi^{2}}\left(R\,|\Lambda|\,R^{-1}\right)^{2}_{\pm} - I\right]\Delta_{\pm}\tilde{E}_{ij},$$

$$\hat{D}_{\xi i\pm1/2j} = \overline{E}_{\xi i\pm1/2j} + \overline{D}_{\xi i\pm1/2j},$$

where

$$minmod(a,b) = \begin{cases} s\times min\left(|a|,|b|\right) & if \quad sign(a)=sign(b)=s \\ 0 & other \end{cases},$$

$$\dot{\boldsymbol{m}}(a,b) = \begin{cases} a & \text{if} \quad |a| \le |b| \\ b & \text{if} \quad |a| > |b| \end{cases}.$$

The second term RHS^{n}_{η} is written similarly.

In approximation of derivatives in convective and diffusion terms, we use second-order central-difference operators.

The numerical solution of the system (7) is calculated in two steps. The first determines the dynamic parameters and second determines the mass species.

Then it is necessary to define Jacobian matrix which, in a case of the thermally perfect gas, represents a difficult task. This problem is connected with the explicit representation of pressure through the unknown parameters. Here pressure is determined by introducing an effective adiabatic parameter of the gas mixture.

$$\overline{\gamma} = \frac{h_{sm}}{e_{sm}}, \tag{14}$$

where

$$h_{sm} = \sum_{i=1}^{N} Y_i \int_{T_0}^{T} c_{p_i} dT$$

and

$$e_{sm} = \sum_{i=1}^{N} Y_i \int_{T_0}^{T} c_{v_i} dT$$

are the enthalpy and internal energy of the mixture minus the heat and energy of formation; $T_0 = 293K$ is the standard temperature of formation, which allows to write an expression for the pressure

$$p = (\overline{\gamma} - 1)\left[E_t - \frac{1}{2}\rho\left(u^2 + w^2\right) - \rho\frac{h_0}{\gamma_\infty M_\infty^2} \right] + \frac{\rho T_0}{M_\infty^2 W}.$$

The temperature is found by using the Newton-Raphson iteration [8-9].

6. Numerical results

The parameters of coordinate transformation (7) have the form:

$$\xi(x) = K + \frac{1}{\tau} arsh\left[\left(\frac{x}{x_c} - 1 \right) sh(\tau K) \right],$$

$$\eta(z) = H\left[(\beta+1) - (\beta-1)\left(\frac{\beta+1}{\beta-1} \right)^{1-\frac{z}{a}} \right] \Bigg/ \left[\left(\frac{\beta+1}{\beta-1} \right)^{1-\frac{z}{a}} + 1 \right],$$

$$K = \frac{1}{2\tau} \ln\left[\left(1 + (e^{\tau} - 1)\frac{x_c}{L} \right) \Bigg/ \left(1 - (e^{\tau} - 1)\frac{x_c}{L} \right) \right],$$

β and τ are refinement factors (β>1 and τ>1), a is the height of the computational domain in the generalized coordinates, and x_c is the point with respect to which grid refinement is performed.

The use of algorithm (13) with the Baldwin-Lomax turbulence model has been tested by authors and results were stated in reference [8].

Numerical simulation was performed for perpendicular injection of a gas into two-dimensional channel with the channel height of - 7,62 cm, length - 15 cm and width of slot 0,0559 cm. The slot was located at a distance of 10 cm from entrance. The parameters were $M_0 = 1$, $T_0 = 642\ K$, $T_\infty = 800\ K$. The pressure ratios ranged from 2.75 to 20, and the freestream Mach number M_∞ ranged from 1.75 to 4.75. The space grid was 241x181. The correction coefficient for compressibility was taken as α =0.3.

The Figure 2 shows the influence of turbulence model on the character of interaction of the jets with the supersonic air flow. In this figure, the shaded pictures of pressure calculated by Baldwin-Lomax and $k-\varepsilon$ turbulence models with and without compressibility correction are represented.

As is well known, the physics flow is the following: due to deceleration of the main flow, the pressure ahead of the jet increases, and a bow shock wave is formed. An oblique shock wave emanates upstream from the bow shock wave. A second shock wave, named the barrel shock emerged behind the oblique shock wave. The bow shock wave, oblique shock wave and barrel shock wave intersect at one point to form a complicated λ-shaped structure.

All of these shock waves are presented in the Figure 2 for different freestream Mach numbers. Although the qualitative picture of the shock waves are similar for both turbulence models, the evident divergence of the λ-shaped structure is observed in the turbulent boundary layer, which is more prominent for smaller M_∞ Figure 2 (a-c).

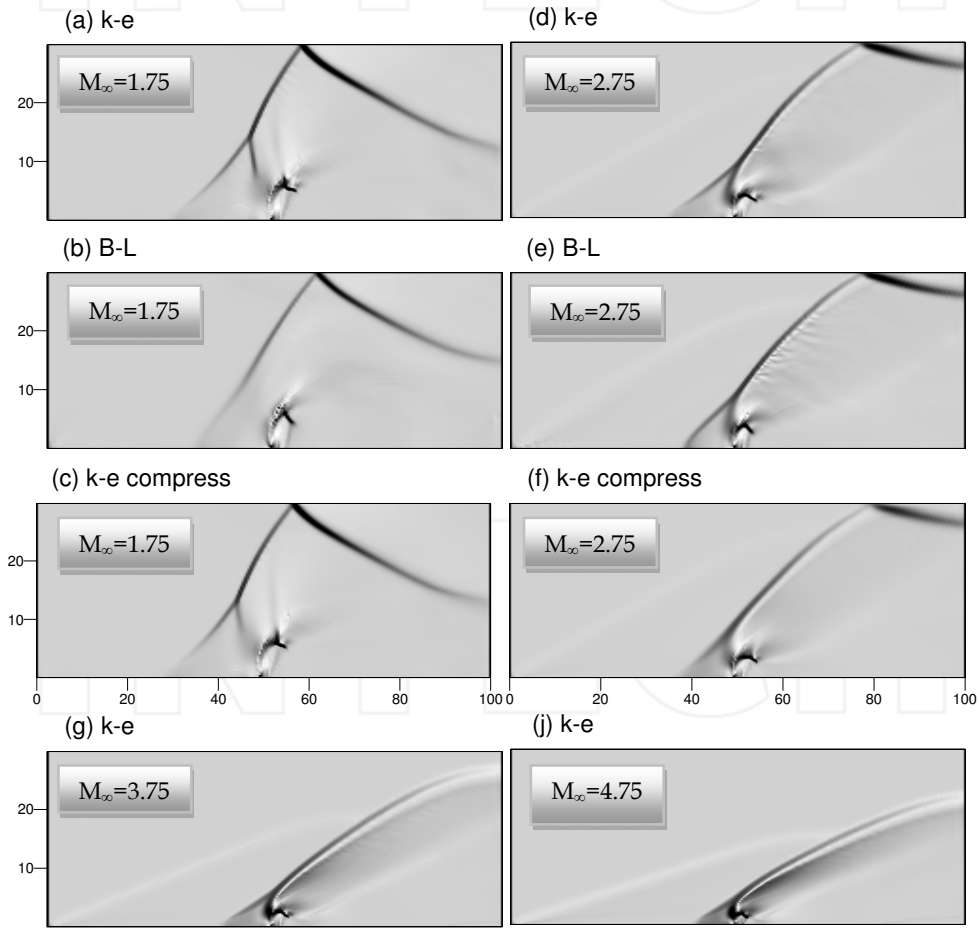

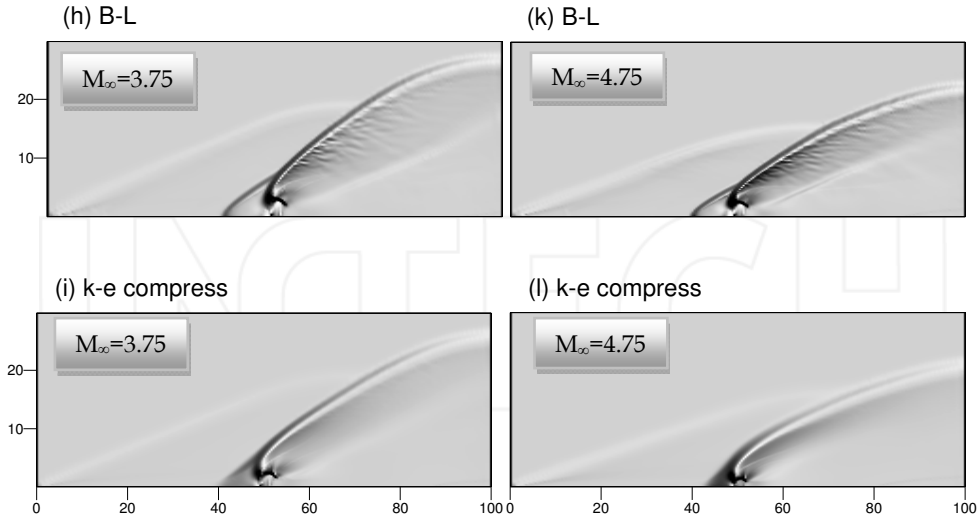

(a)–(c) $M_\infty = 1.75$, (d)–(f) $M_\infty = 2.75$
(g)–(i) $M_\infty = 3.75$, (j)–(l) $M_\infty = 4.75$

Fig. 2. Shaded picture of pressure for various Mach number with $k-\varepsilon$, B-L, and $k-\varepsilon$ compressibility turbulence models

The differences among the models in the boundary layer are also evident in the local Mach number contours. The distribution of the iso-Mach line contours is shown in Figure 3. In all cases the sonic velocity of the jet becomes supersonic at a certain distance because of the acceleration immediately after injection. Then, the boundary of the supersonic region is closed, forming a barrel which is a consequence of interaction of the shock waves system in the jet itself. With increasing freestream Mach number the jet penetration is reduced, due to the reduction of the hydrogen momentum with respect to the incoming air momentum and consequently a significant decrease in the barrel size is observed. The iso-Mach line contours in the subsonic region (Figure 3) were compared, and quantitative differences among the models can be seen. It is obvious that increasing of M_∞ reduces these differences.

The numerical experiments have shown that the acceleration of the flow inside of the barrel is larger for the $k-\varepsilon$ model than for the algebraic model. For example, in the case of $k-\varepsilon$ model the flow inside of the barrel for $M_\infty = 1.75$ is accelerated until the maximum local Mach number becomes $M = 3.4$ whereas in the algebraic model the local Mach number only reaches $M = 2.8$. Simulations that used different values of M_∞ revealed that the acceleration of both models is decreased with increaseed Mach number; for the case of $M_\infty = 4.75$ for $k-\varepsilon$ model maximum inside of barrel is $M = 2.87$ and for algebraic $M = 2.56$.

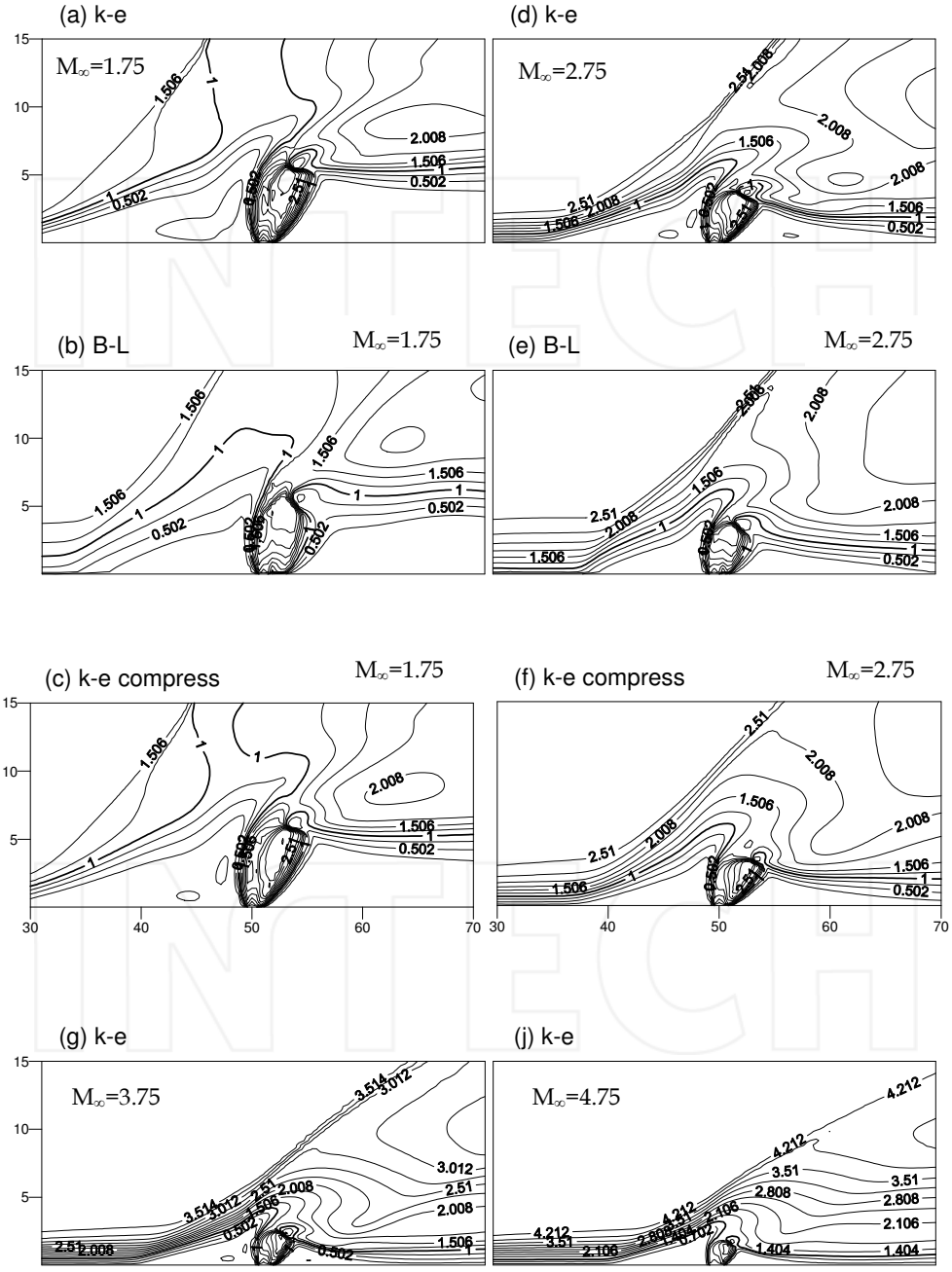
(a) k-e
M∞=1.75
(d) k-e
M∞=2.75
(b) B-L
M∞=1.75
(e) B-L
M∞=2.75
(c) k-e compress
M∞=1.75
(f) k-e compress
M∞=2.75
(g) k-e
M∞=3.75
(j) k-e
M∞=4.75

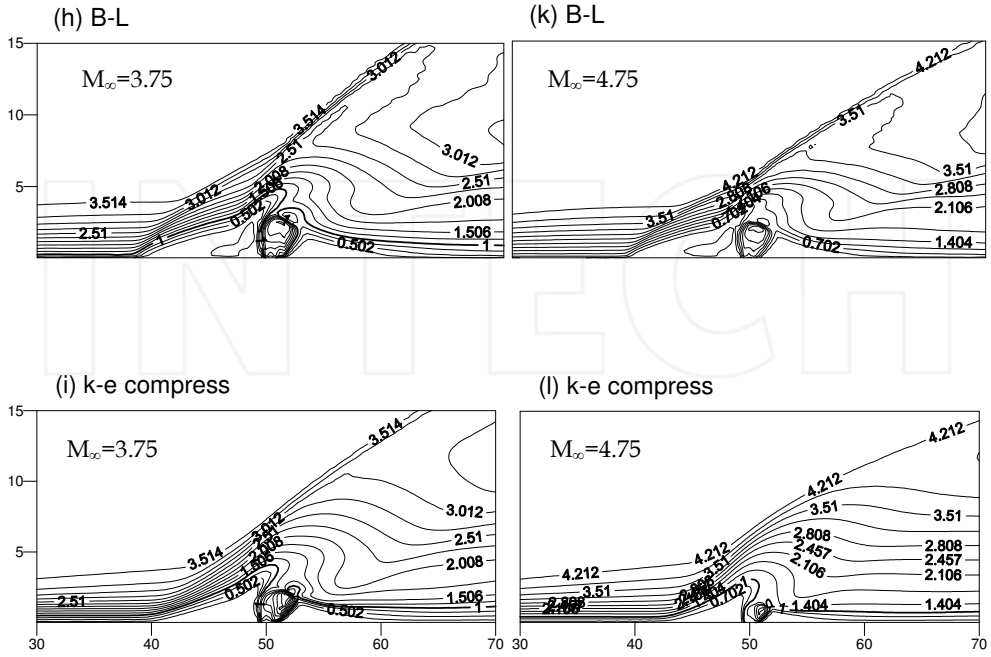

(a)–(c) $M_\infty = 1.75$, (d)–(f) $M_\infty = 2.75$
(g)–(i) $M_\infty = 3.75$, (j)–(l) $M_\infty = 4.75$

Fig. 3. iso-Mach line contours for various Mach number with $k-\varepsilon$, B-L, and $k-\varepsilon$ compressibility turbulence models

The observed differences among the models are confirmed by Figure 4, where the boundary layer separation distance from the jet is shown as a function of Mach number. In the case of taking into account compressibility effect (Figure 4, line 3) the curve of the separation distance is located between $k-\varepsilon$ and Baldwin-Lomax model lines. The curves show that the sizes of counter-rotating primary and secondary upstream vortices in the region upstream of the jet differ.

Fig. 5. (a-k) shows contours of the constant mass concentrations of hydrogen for different M_∞. The penetration and mixing of hydrogen is performed in accordance with the physics of flows, consequently the depth of penetration hydrogen grows with increased M_∞.

Contour plots of turbulent characteristics of the flow are shown in Figures 6 and 7. Figure 6 shows comparison of turbulence kinetic energy k with turbulence energy dissipation ε calculated by $k-\varepsilon$ model for various freestream Mach numbers, while Figure 7 shows the same comparison computed with the $k-\varepsilon$ compressibility model.

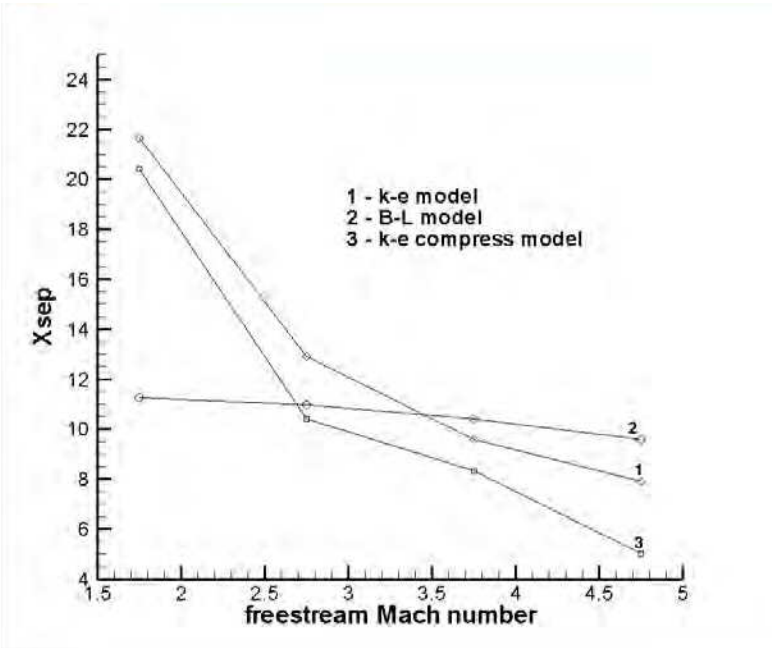

Fig. 4. Separation length as a function of freestream Mach number.

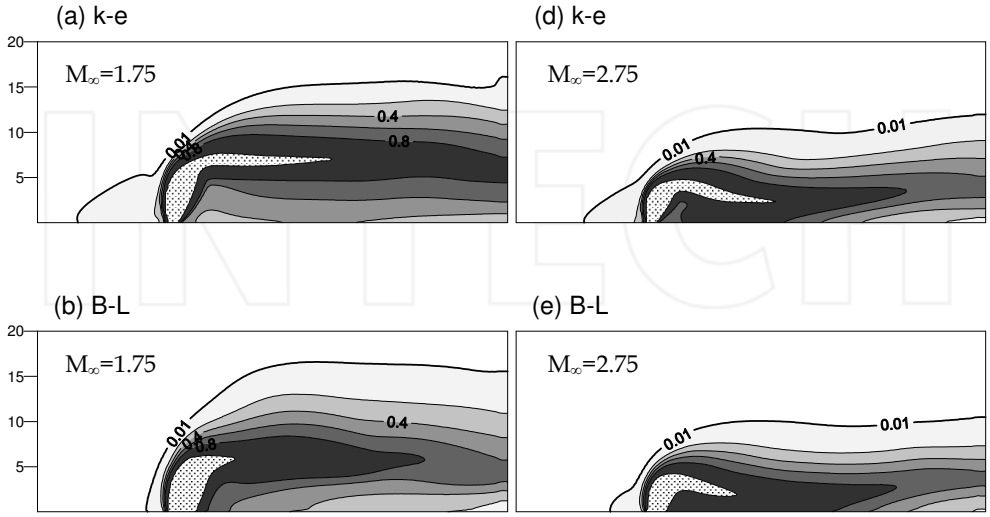

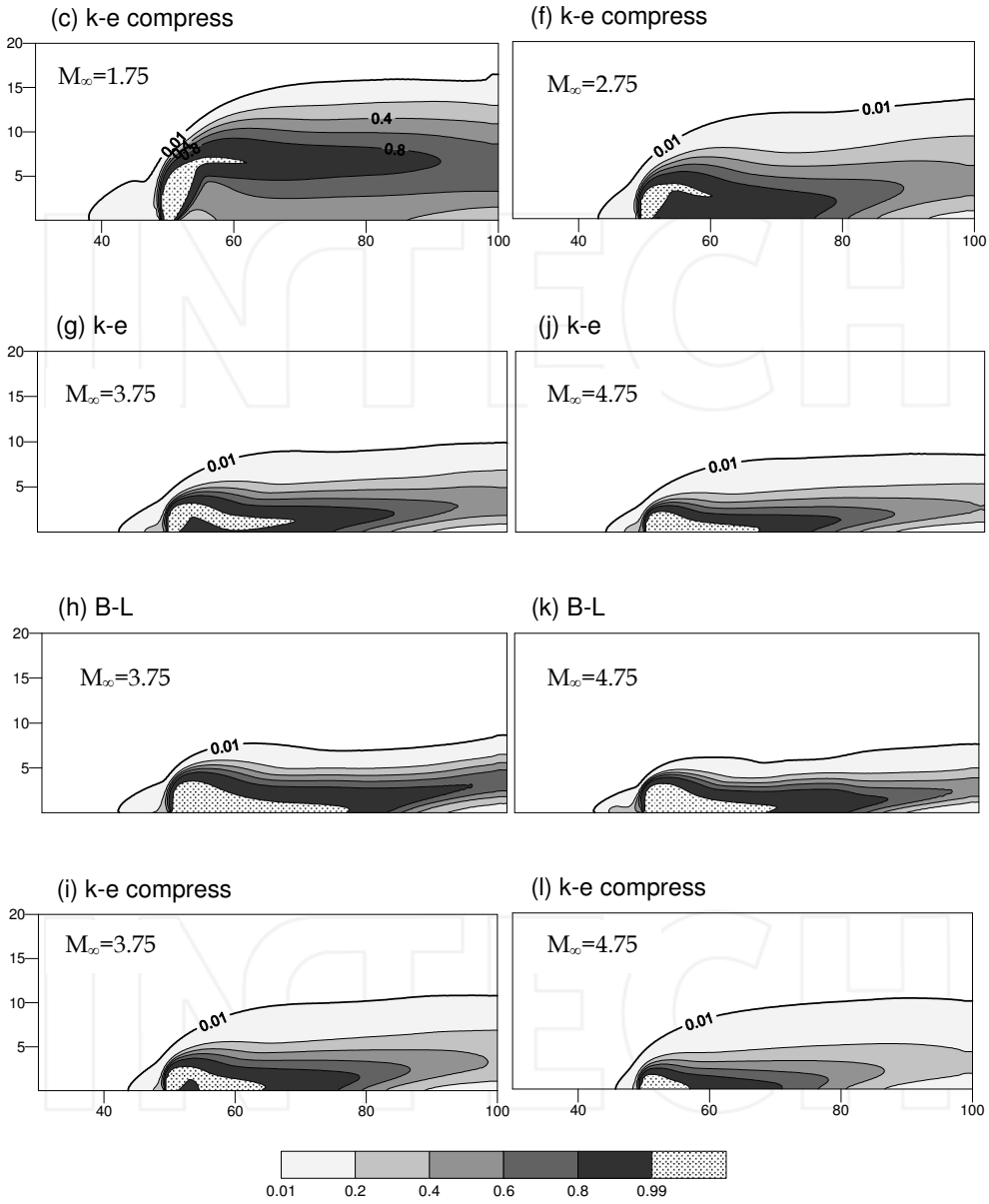

(a)-(c) $M_\infty = 1.75$, (d)-(f) $M_\infty = 2.75$

(g)-(i) $M_\infty = 3.75$, (j)-(l) $M_\infty = 4.75$

Fig. 5. Mass fraction contour of hydrogen.

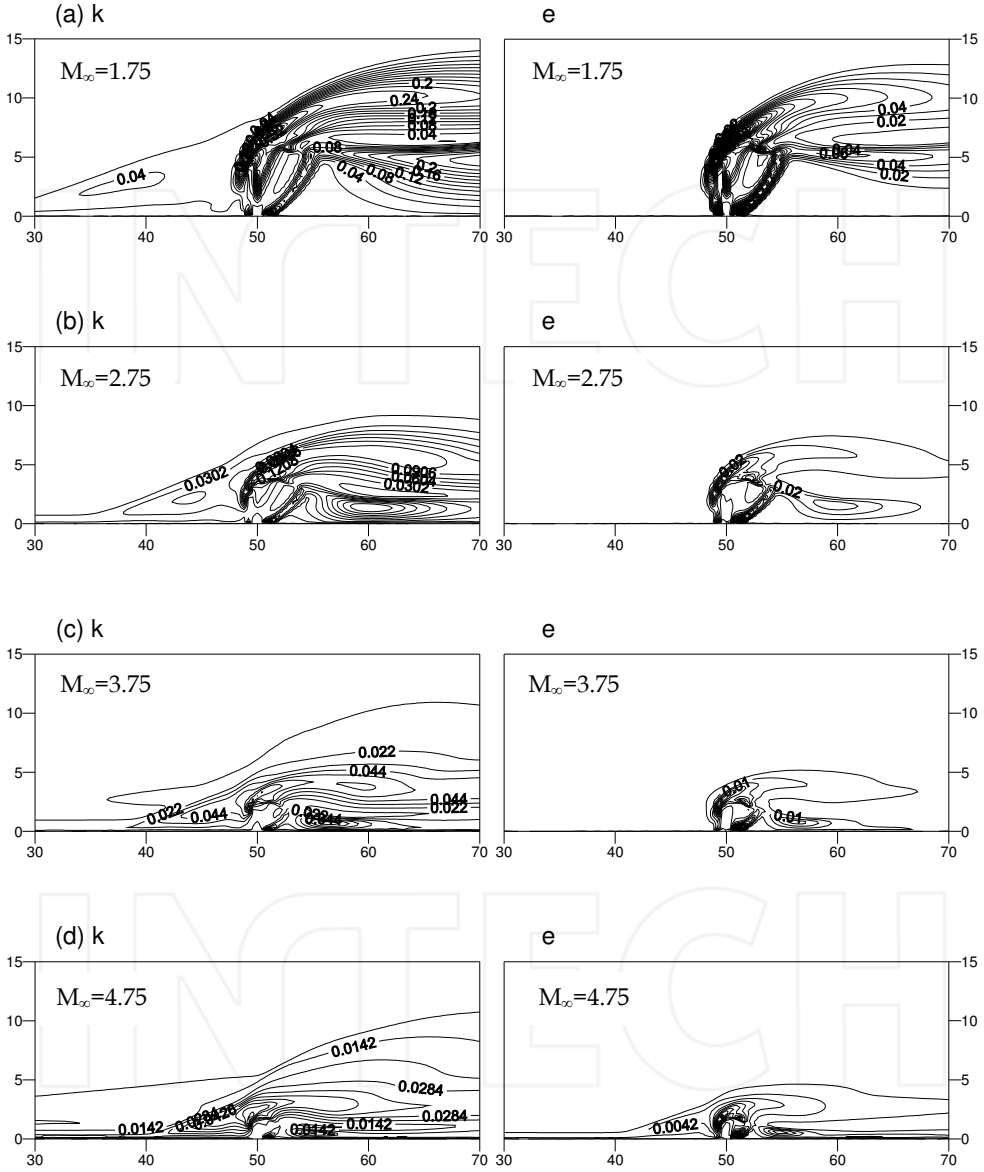

Fig. 6. Comparison of $k-\varepsilon$ contours for various freestream Mach numbers, calculated by the $k-\varepsilon$ model.

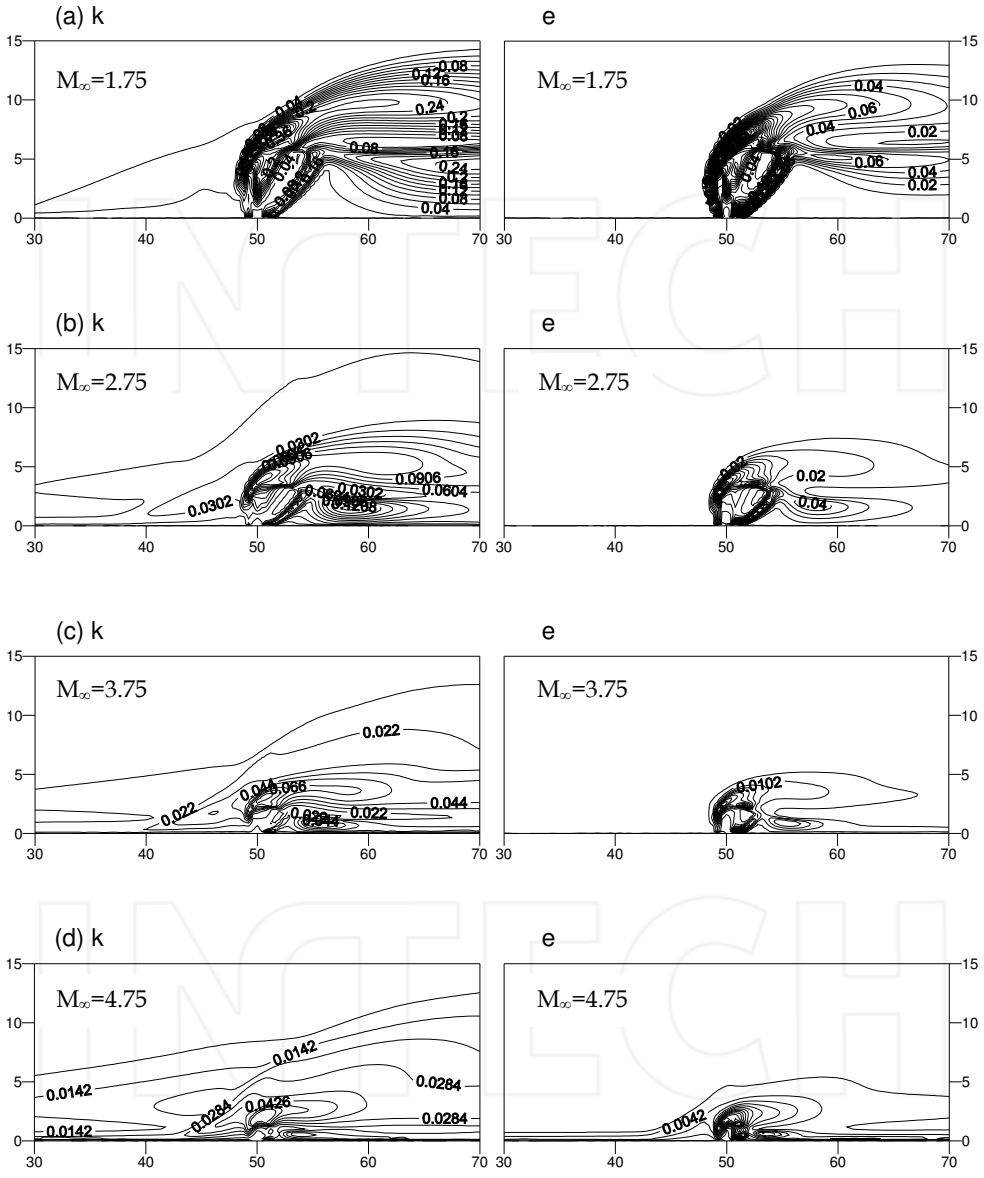

Fig. 7. Comparison of $k-\varepsilon$ contours for various freestream Mach numbers, calculated by the $k-\varepsilon$ compressibility model.

The dynamics of reduction of dimensionless residual norm of gas density for the implicit method is shown in the Figure 8. The figure shows that increasing the subsonic zones (smaller M_∞) degrades the convergence. Apparently, numerical simulation with smaller of M_∞ will need optimization in order to provide better convergence.

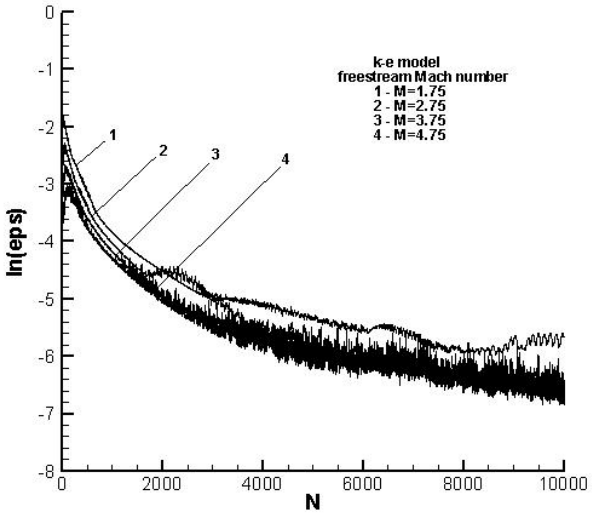

(a)

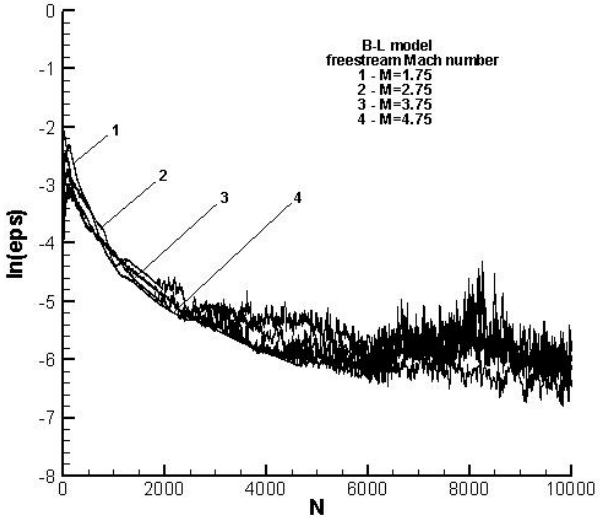

(b)

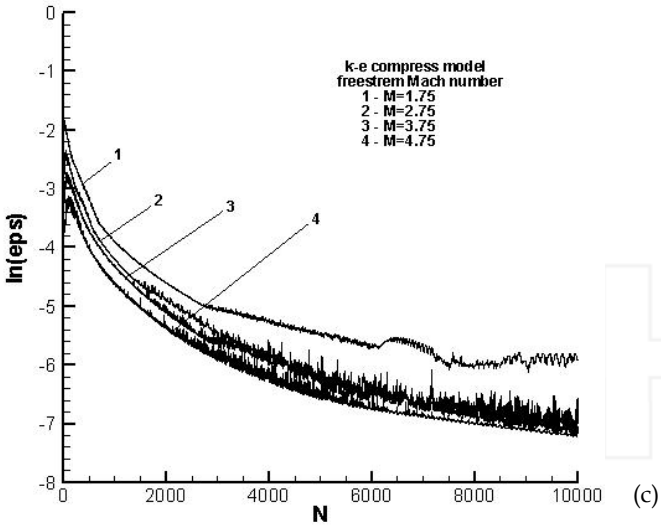

Fig. 8. Dimensionless residual norm for the gas density vs. the number of iterations (a)- $k-\varepsilon$ model, (b)–B-L model, (c)- $k-\varepsilon$ compressibility model.

The influence of the pressure ratio on the upstream flow structure was also studied. An analysis of the influence of the jet pressure ratio on the bow shock wave shows that the angle of inclination of the latter increases with increasing pressure ratio behind the shock wave and ahead of it. The effect of the jet pressure ratio on the separation-region length is illustrated in Figure 9 for $M_\infty = 3.75$. Here results are represented which were calculated by the convergence of the dimensionless residual norm for gas density $\ln\varepsilon$ = -5.

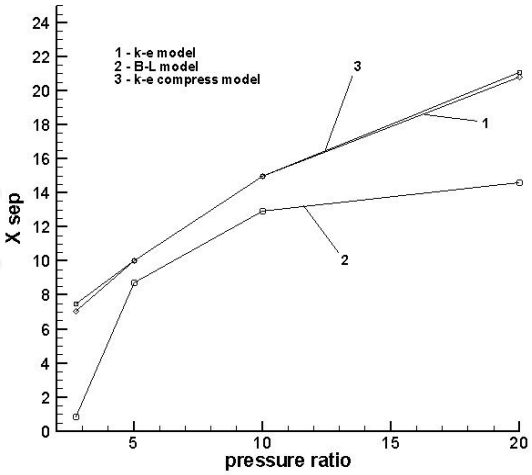

Fig. 9. Separation length as a function of static pressure ratio.

7. Conclusion

In the present work, the numerical model and computer code have been developed for a $k-\varepsilon$ turbulent model that includes compressibility correction to simulate turbulent supersonic air flow with transfer injection of the hydrogen from slots of the walls. The numerical method is based on the ENO scheme.

Comparison is made between solution by using algebraic Baldwin-Lomax's turbulence model and $k-\varepsilon$ model. The influence of the compressibility effect on the shock wave structure is studied.

The interaction of the supersonic air flow with transfer injection of jets depending on the freestream Mach number and pressure ratio have been studied. In spite of similarity in the shock wave structure for both turbulence model, the numerical experiments have shown that the sizes of counter-rotating primary and secondary upstream vortices in the region upstream of the jet differ.

The developed computer code allows to study of mixing flowfield behavior with various injector geometries and reacting flows which is important problems in the design of supersonic combustion ramjet (scramjet) engines.

8. References

[1] Drummond J. P. and Weidner E. H., "Numerical Study of a Scramjet Engine Flowfield", AIAA Journal, Vol. 20, No.9, 1982, pp. 1182-1187.

[2] Weidner E. H. and Drummond J. P., "Numerical Study of Staged Fuel Injection for Supersonic Combustion", AIAA Journal, Vol. 20, No.10, 1982, pp. 1426-1431.

[3] Clarence F. Chenault and Philip S. Beran, "k-e and Reynolds Stress Turbulence Model Comparisons for Two-Dimensional Injection Flows", AIAA Journal, Vol. 36, No. 8, 1998, pp. 1401-1412.

[4] Grasso F. and Magi V., "Simulation of Transverse Gas Injection in Turbulent Supersonic Air Flows", AIAA Journal, Vol. 33, No. 1, 1995, pp. 56-62.

[5] Mohammad Ali, Toshi Fujiwara, Joseph E. Leblanc, "Influence of main flow inlet configuration on mixing and flameholding in transverse injection into supersonic airstream", International Journal of Engineering Science, 2000, pp. 1161-1180.

[6] Mohammad Ali, S. Ahmed, A. K. M. Sadrul Islam, "The Two-Dimensional Supersonic Flow and Mixing with a Perpendicular Injection in a Scramjet Combustor", Journal of Thermal Science, Vol. 12, No.4, 2003, pp. 372-380.

[7] Shuen J. S. and Yoon S., "Numerical Study of Chemically Reacting Flows Using a Lower-Upper Symmetric Successive Overrelaxation Scheme", AIAA Journal, Vol. 27, No. 12, 1989, pp. 1752-1760.

[8] P. Bruel and A. Zh. Naimanova, "Computation of the normal injection of a hydrogen jet into a supersonic air flow", Thermophysics and Aeromechanics, Vol.17, No. 4, 2010, pp. 531-542.

[9] Beketaeva A.O., Naimanova A.Zh. Numerical simulation of a supersonic flow with transverse injection of jets // Journal of Applied Mechanics and Technical physics, 2004. Vol.45, №3. P.367-374.

[10] D. P. Rizzetta (1995) Numerical Investigation of Supersonic Wing-Tip Vortices. 26th AIAA Fluid Dynamics Conference.

[11] Rizzetta D.P., "Numerical Simulation of Slot Injection into a Turbulent Supersonic Stream", AIAA Journal, Vol.30, No.10, 1992, pp. 2434-2439.

[12] Kee R.J., Rupley F.M., Miller J.A. CHEMKIN-II: a Fortran chemical kinetic package for the analysis of gas-phase chemical kinetics // SANDIA Report SAND89-8009. – 1989.

[13] J. O. Hirschfelder, Ch. F. Curtiss, R. B. Bird, "Molecular Theory of Gases and Liquids", Moscow, 1961.

[14] Dean R. Eklund and J. Philip Drummond, NASA Langley Research Center, Hampton, Virginia and H.A. Hassan, North Carolina State University, Raleigh, North Carolina. Calculation of Supersonic Turbulent Reacting Coaxial Jets // AIAA Journal. Vol.28, NO.9, September 1990.

[15] SUN De-chuan, HU Chun-bo, CAI Ti-min. Computation of Supersonic Turbulent Flowfield with Transverse Injection // Applied Mathematics and Mechanics. English Edition. Vol.23, No 1, Jan 2002. P. 107-113.

[16] Kee R.J., Rupley F.M., Miller J.A. CHEMKIN-II: a Fortran chemical kinetic package for the analysis of gas-phase chemical kinetics // SANDIA Report SAND89-8009. – 1989.

[17] Harten A., Engquist B., Osher S., Chakravarthy S.R. Uniformly High Order Accurate Non-oscillatory Schemes, III // Journal of Computational Physics. – 1987. – Vol.71. – P.231-303.

[18] Harten A., Osher S., Engquist B., Chakravarthy S.R. Some Results on Uniformly High-Order Accurate Essentially Non-oscillatory Schemes // Applied Num. Math. – 1986. – Vol.2. – P.347-377.

Advanced Methods for Practical Applications in Fluid Mechanics

Edited by Prof. Steven Jones

ISBN 978-953-51-0241-0
Hard cover, 230 pages
Publisher InTech
Published online 14, March, 2012
Published in print edition March, 2012

Whereas the field of Fluid Mechanics can be described as complicated, mathematically challenging, and esoteric, it is also imminently practical. It is central to a wide variety of issues that are important not only technologically, but also sociologically. This book highlights a cross-section of methods in Fluid Mechanics, each of which illustrates novel ideas of the researchers and relates to one or more issues of high interest during the early 21st century. The challenges include multiphase flows, compressibility, nonlinear dynamics, flow instability, changing solid-fluid boundaries, and fluids with solid-like properties. The applications relate problems such as weather and climate prediction, air quality, fuel efficiency, wind or wave energy harvesting, landslides, erosion, noise abatement, and health care.

How to reference

In order to correctly reference this scholarly work, feel free to copy and paste the following:

Ye. Belyayev and A. Naimanova (2012). Two-Dimensional Supersonic Flow with Perpendicular Injection of the Gas, Advanced Methods for Practical Applications in Fluid Mechanics, Prof. Steven Jones (Ed.), ISBN: 978-953-51-0241-0, InTech, Available from: http://www.intechopen.com/books/advanced-methods-for-practical-applications-in-fluid-mechanics/two-dimensional-supersonic-flow-with-perpendicular-injection-of-the-gas

INTECH
open science | open minds

InTech Europe
University Campus STeP Ri
Slavka Krautzeka 83/A
51000 Rijeka, Croatia
Phone: +385 (51) 770 447
Fax: +385 (51) 686 166
www.intechopen.com

InTech China
Unit 405, Office Block, Hotel Equatorial Shanghai
No.65, Yan An Road (West), Shanghai, 200040, China
中国上海市延安西路65号上海国际贵都大饭店办公楼405单元
Phone: +86-21-62489820
Fax: +86-21-62489821